DEVELOPMENT OF GALLIUM ALUMINUM PHOSPHIDE

ELECTROLUMINESCENT DIODES

by

R. J. Chicotka
M. R. Lorenz
A. H. Nethercot
G. D. Pettit

July 7, 1972

NATIONAL AERONAUTICS AND SPACE ADMINISTRATION

TABLE OF CONTENTS

DEVELOPMENT OF GALLIUM ALUMINUM PHOSPHIDE

ELECTROLUMINESCENT DIODES

By R. J. Chicotka, M. R. Lorenz, A. H. Nethercot and G. D. Pettit

INTRODUCTION

The objective of this report is to describe the work done under Contract NAS 1-11037 between July 8, 1971 and July 7, 1972 on the development of gallium aluminum phosphide alloys for electroluminescent light sources. It will broadly cover the preparation of this wide band gap semiconductor alloy, its physical properties (particularly the band structure, the electrical characteristics, and the light emitting properties) and work done on the fabrication of diode structures from these alloys.

A chief motivation of this work was that, in order to improve the visibility of electroluminescent diodes, it is important that the light emitted have a frequency closely matching that at which the human eye has its maximum sensitivity. This can be accomplished in an optimum fashion by using a semiconductor material which has a band gap substantially larger than this frequency and which can be doped with efficient radiative recombination centers to which the injected carriers will be fairly deeply bound such that the emitted light has this optimum frequency. One such material is the ternary alloy (Ga,Al)P. In addition to the interest in the light emitting properties of this material, little was previously known about its basic chemical and physical properties, the behavior of dopants, and the difficulties involved in fabricating devices and device structures.

GROWTH TECHNIQUES AND RESULTS

Epitaxial layers of (GaAl)P have been grown on GaP substrates by a liquid phase epitaxy technique. Compositional control and reproducibility of the epilayers were obtained through the use of a special liquid phase epitaxy apparatus, the main features of the apparatus being: a special wiping shoulder (Fig. 1) to remove the melt after the epilayer is grown and before cooling to room temperature; also the melt is contained in such a way that only a small amount is needed to form a uniform layer of liquid solution over the substrate. The ability to intentionally dope or counterdope by either adding dopant to the melt or by using separate melt and source materials is inherent in the apparatus design (Fig. 2).

A cross section diagram of the apparatus used is shown in Fig. 1. The GaP substrate is held stationary in a recess cut into the top surface of a graphite holder; the source material (either intentionally doped or nominally undoped GaP) is similarly held within another recess. The melt, containing the

gallium, aluminum and any necessary dopant, rests above the source material within the hole in the sliding plate number 2, held flat under pressure from plate number 1. Plate number 1 can be designed to contain covered compartments which can be used for such dopants as tellurium or zinc to grow built-in junctions. Plate number 2 can be designed to accommodate another source material and melt to the left of the substrate thus enabling two distinct counterdoped epilayers to be grown onto the substrate. In the present implementation, the number 2 plate contains a single source and melt recess and moves the melt back and forth in a push-pull mode of operation.

The furnace is designed so that there is a slight vertical temperature gradient, approximately 2°C per cm, the temperature being slightly higher at the top of the apparatus. There is essentially no temperature gradient across the holder horizontally. This ensures that most of the material is deposited on the surface of the substrate, and that spontaneous or spurious nucleation within the melt is held to a minimum. The thinness of the melt above the substrate should also substantially reduce the possibility of precipitating species being deposited anywhere but on the substrate.

When using this technique and apparatus, the following experimental procedure is used. The graphite apparatus is loaded with the GaP substrate, source material, and gallium-aluminum melt (sufficient source material is added to ensure that the melt will be saturated and that some of the source material will be left remaining in the recess). The graphite holder is positioned in the cool end of a mechanically sealed quartz liner by a taper joint which protrudes from the furnace. An argon flow of approximately 130 cc/min is passed through the liner for approximately 15 minutes to remove any air that might have leaked into the system. The argon flow is then reduced to approximately 40 cc/min and the graphite holder is slid into the hot zone of the furnace and carefully positioned within the isothermal zone. The holder is heated to such a temperature that the melt is saturated with the source material. For a typical $Ga_{1-x}Al_xP$ run, the temperature is about 1150°C. The melt is then moved by plate number 2 over the substrate where an epitaxial layer is grown by cooling the solution. Typical cooling rates of 0.76°C/min are used and approximately 30 microns of $Ga_{1-x}Al_xP$ can be grown over a 60°C temperature interval. The melt is then wiped off the surface of the wafer by moving the number 2 plate to a position midway between the substrate and source recesses, thus leaving a smooth-surfaced melt-free epitaxial layer on the substrate. The layers grown by this process are generally uniform in thickness throughout because of the very small horizontal temperature gradient and the confinement of the melt to a thin layer above the substrate.

A design modification in the apparatus permitting the use of two independent melts for the growth of p-n junctions is shown schematically in Fig. 2 and will be referred to in the last section of this report.

The majority of the grown epilayers wiped clean after growth; however a few did not and some wiped only partially clean, leaving a small amount of melt on the surface. Growth from this remaining melt then continued as the holder was brought to room temperature until most of the GaP and Al in solution was exhausted by either depositing on the substrate or appearing as spurious

crystallites precipitated from solution. The usual reason for the epilayer not wiping entirely clean is due to edge growth, i.e., formation of a layer on the periphery of the substrate that is thicker than the layer on the planar surface of the substrate. This either inhibits or entirely prevents the sliding and wiping motion of plate number 2. This edge growth is in the 111 direction on a 100 oriented wafer and growth in the 111 direction is more rapid than in the 100 direction. This was eliminated entirely by growth on a 111 oriented wafer.

A tabulation of all the liquid phase epitaxy growths made using this process is given in Table 1. In column form are tabulated the parameters for the various epilayer growths made, including the GaP substrate orientations and electrical type, and the amount of gallium, aluminum and GaP source material used in each run. Growth temperature and temperature span are respectively the temperature at which the source material and melt was equilibrated and the temperature interval over which growth took place. This Table includes information from the three major phases of the experimental program: The (GaAl)P epilayers numbered GLPE-1 through 25 inclusive were grown to establish the compositional dependence of the alloy system on temperature and the variation of the aluminum solubility in the liquid and solid phases. Epilayers numbered 26 to 63 inclusive were grown to establish the variations in the electrical properties as a function of different impurities and growth conditions. Finally, epilayers numbered 64 and on were grown to fabricate p-n junction diodes.

The solubility of GaP in Ga for two temperatures of growth and for various aluminum to gallium ratios was determined by weight loss of the source material. The solubility of GaP in Ga as a function of the Al concentration in the melt at $1100°C$ and at $1150°C$ is shown in Fig. 3. The solubility of GaP in Ga is plotted against gm Al/gm Ga. Points located on the axis where there is no aluminum in the melt were obtained from previously determined solubility curves of Ga versus GaP. At both temperatures, the solubility of GaP depends qualitatively as expected upon the amount of Al present.

The alloy composition variable X in $Ga_{1-x}Al_xP$ and its dependence on the aluminum concentration in the melt is shown in Fig. 4. Here we have plotted the mole fraction X in the solid against the composition of aluminum in the melt for the growth temperature of $1150°C$. These points and their errors were determined by extrapolating the composition versus distance curves in Fig. 5 (described below) to zero distance from the substrate. A smooth curve has been drawn through all the points. Thus we have determined the solid-liquid compositional relationship for the $1150°C$ isotherm.

The epitaxial overgrowths were analyzed for composition by the electron microprobe technique. Samples were analyzed for surface composition and variations in surface composition. Cross sections of the overgrowth were also analyzed to determine the composition gradient within the epitaxial layer. In Fig. 5 we have plotted the composition variable X in $Ga_{1-x}Al_xP$ for some of the epitaxial layers against distance as measured from the substrate towards the surface. The omission of data in the $0-8\mu$ region is due to the effects of the GaP substrate. Also, the data tends to become unreliable near the free surface where the electron beam is not totally within the confines of the sample.

It is evident that as the aluminum concentration in the melt decreases the composition in the alloy shifts to lower aluminum concentrations. For epilayers grown with the same aluminum to gallium ratio in the melt, the alloy composition reproduces to within 2%. Also the concentration gradients within these samples are very similar. Samples grown under similar conditions were GLPE-15, 16 and GLPE-17, 21 and GLPE-22, 24.

From the data shown we see that the composition is fairly uniform for the overgrowths with the maximum changes in composition occurring in the last few microns of overgrowth adjacent to the free surface. A rapid decrease in the aluminum composition near the free surface can be noted in some samples. This sharp gradient near the surface in most cases can be ascribed to a layer of solidified melt, this material being left on the surface after wiping the melt from the surface. This was clearly the case for samples 17, 21, 22 and 25. The compositions believed to correspond to this growth from the unwiped melt are shown in Fig. 5 as the dashed extensions.

More complete microprobe measurements of the surface composition as well as the variations in the surface composition are presented in Table 2. For the majority of the samples the surface composition lies within the limits of the alloy composition as determined by analysis of the cross sections. However, some of the alloys with higher Al concentrations differ significantly from the microprobe data obtained from the cross sections. The surface compositions of these samples are all higher than the composition limits in the cross section and these surface compositions tend to centralize in the range $0.87 < x < 0.92$.

The reasons why this occurs are not obvious. However, it should be noted that, with the exception of GLP-18, all the samples which show this anomalous surface concentration were from the early series GLP-1 through 7 and that these samples were almost all more aluminum rich than the samples with a more normal surface concentration. It is possible that surface oxidation of these more aluminum rich samples is in part responsible for this anomalous effect.

Thus, from the microprobe data taken on both the cross sections and the layer surfaces we can conclude that good control over the composition and composition gradient has been obtained and that the results are quite reproducible.

TABLE I

GALLIUM ALUMINUM PHOSPHIDE

GLPE	Substrate	(Ga(gm)	Al(mg)	GaP(mg)	Dopant(mg)	Source Time hr	Growth Temp °C	Temp Span °C	Growth Rate °C/min	Thickness (microns)
1	111B s.i	2.5	31.5	30	none	1/2	1100	60	0.82	< 10
2	111B s.i.	2.5	31.2	--	none	1	1101	61	0.4	0-10 - no good
3	100 p	2.5	31.0	26	none	1/2	1099	59	0.76	9.5 - bad spot
4	100 p	2.5	31.3	29	none	1	1099	59	0.36	7-8
5	100 p	2.5	31.4	30	none	1/2	1098	58	0.75	8-8.7
6	100 p	2.5	31.0	28	none	1/2	1100	30	0.77	> ~ 6
7	100 p	2.5	31.7	25	none	1/2	1100	60	1.62	> 10.5
8	100 p	2.5	21.0	16.3	none	1/2	1100	30	0.73	poor
9	100 p	2.5	20.5	14.1	none	1/2	1100	32	0.76	no growth
10	100 p	2.5	11.3	48.7	none	1/2	1099	30	0.73	10.4
11	100 p	2.5	20.9	33.7	none	1/2	1100	76	0.76	15.7
12	100 n	7.5	91	103.7	none	1/2	1120	80	0.77	19.1
14	100 n	7.5	91	134.3	none	1/2	1150	100	0.78	30
15	100 n	7.5	60.1	>105.6	none	1/2	1150	100	0.78	34-35
16	100 n	7.5	60.6	178.9	none	1/2	1150	100	0.78	37.4
17	100 n	7.5	30.6	289.8	none	1/2	1150	100	0.78	39-42
18	100 n	7.5	91.3	136.1	none	1/2	1150	100	0.77	22.6-25
19	100 n	7.5	60.1	175.9	none	1/2	1150	100	1.67	23
20	100 n	7.5	60.0	186.9	none	1/2	1150	75	0.076	52
21	100 n	7.5	30.14	289.7	none	1/2	1150	113	0.74	42
22	100 n	7.5	15.08	>401.1	none	1/2	1150	62	0.75	38.3
23	100 n	7.5	0	>479.9	none	1/2	1150	60	0.75	0
24	100 n	7.5	15.13	433.1	none	1/2	1150	60	0.76	60-80
25	100 n	7.5	45.97	211.1	none	1/2	1150	60	0.76	38-47

TABLE I (continued)

GALLIUM ALUMINUM PHOSPHIDE

GLPE	Substrate	Ga (gm)	Al (mg)	GaP (mg)	Dopant (mg)	Container	Growth Temp. °C	Temp. Span °C	Growth Rate °C/min.	Thickness (microns)
26	100 p	5.0	29.8		none	BN	1151	60	0.77	29-30
27	100 p	5.0	29.6	147.3	none	BN	1150	60	0.76	31-33
28	100 p	5.5	32.9	166.9	TE 10	BN	1150	60	0.78	33
29	100 p	5.5	33.3	183.5	TE 50	BN	1151	61	0.78	33-39
30	100 p	5.5	33.1	161.7	S 1	BN	1151	61	0.76	31-37
31	100 p	6.0	36.3	173.9	S 0.2	BN	1150	60	0.76	38-42
32	100 p	5.75	34.9	164.7	none	BN	1150	65	0.76	33-35
33	100 p	5.5	33.2	175.1	TE 101	BN	1150	60	0.76	38
34	100 p	5.5	33.1	163.4	TE 10	BN	1150	60	0.76	34-38
35	100 p	5.5	33.1	162.6	TE 1	BN	1150	61	0.76	30
36	100 p	5.5	33.2	167.5	C 0.3	BN	1149	67	0.77	28-32
37	100 s.i.	5.5	32.9	165.5	none	BN	1151	61	0.77	21-31 - poor
38	100 s.i.	5.5	33.1	160.4	none	BN	1149	59	0.76	poor
39	100 n	5.5	33.9	161.4	Zn 51	BN	1150	60	0.75	24
40	100 n	5.5	33.1	163.5	Zn 10	BN	1150	63	0.76	22-26
41	100 n	5.5	33.7	162.7	Zn 2.3	BN	1151	61	0.75	23
42	111B s.i.	5.5	33.4	162.1	none	BN	1151	61	0.76	oxidized 17
43	111B s.i.	5.5	33.5	168.3	none	BN	1150	60	0.76	22-24
44	111A s.i.	5.5	32.9	174.4	Zn 58	BN	1149	60	0.76	25-26
45	111A s.i.	5.5	33.2	169.2	TE 11	BN	1150	60	0.76	25-28

TABLE I (continued)

GALLIUM ALUMINUM PHOSPHIDE

GLPE	Substrate	Ga (gm)	Al (mg)	GaP (mg)	Dopant (mg)	Container	Growth Temp. °C	Temp. Span °C	Growth Rate °C/min.	Thickness (microns)
46	100 n	5.5	33.4	165.2	TE 3.5	BN	1150	61	0.76	22-26
47	111A s.i.	5.5	none	387.8	none	BN	1100	61	0.74	60
48	111A s.i.	5.5	33.3	156.3	none	BN	1150	60	0.77	30
49	111A s.i.	5.5	33.1	202.8	none	BN	1151	59	0.77	25-30
50	111A s.i.	5.5	33.5	160.6	none	BN	1151	61	0.75	24-30
51	111A s.i.	5.5	33.5	163.5	none	BN	1152	62	0.77	26-29
52	111A s.i.	7.5	45.5	215.9	none	Graphite	1150	60	0.77	30
53	111A s.i.	5.5	33.3	173.3	none	BN	1151	61	1.7	28-33
54	111B s.i.	5.5	32.9	165.7	none	BN	1151	61	0.76	25-28
55	111A s.i.	5.5	16.2	259.9	none	BN	1151	55	0.76	34
56	111A s.i.	7.5	33.5	163.1	none	BN	1150	60	0.76	no good
57	111A s.i.	7.5	45.6	217.5	none	Graphite	1152	62	0.76	25-29
58	111A s.i.	7.5	45.0	219.4	none	Graphite	1152	62	0.76	26
59	111A s.i.	7.5	45.5	213.3	Si 1.4	Graphite	1151	61	0.76	26
60	111 p	7.5	45.6	212.3	TE 8.8	Graphite	1151	49	0.75	28
61	111 p	7.5	45.1	212.9	TE 10.7	Graphite	1150	60	0.76/~50	47-60
62	111 s.i.	7.5	45.8	214.6	TE 10.4	Graphite	1150	60	2.0	19-24
63	111 n	7.5	45.5	210.7	TE 11	Graphite	1150	60	2.0/0.8	20-25
64	111 s.i.	7.5	44.87	213.6	none	Graphite	1150	60	2.2	19-20
65	111 n	7.5	45.14	212.3	TE 11.6	Graphite	1150	60	2.2/0.8	22

TABLE I (continued)

GALLIUM ALUMINUM PHOSPHIDE

GLPE	Substrate	Ga (gm)	Al (mg)	GaP (mg)	Dopant (mg)	Container	Growth Temp. °C	Temp. Span °C	Growth Rate °C/min	Thickness (microns)
66	111 n	7.5	45.19	209.0	TE 5.6	Graphite	1150	70	2.2/0.8	26
67	111 s.i.	7.5	45.02	213.2	none	Graphite	1150	60	0.76	28
68	111 n	7.5	45.71	207.0	TE 12.9	Graphite	1150	62	2.2/0.8	24
69	111 s.i.	7.5	45.4	204.1	none	Graphite	1150	60	0.76	26
70	111 n	7.5	45.3	213.6	TE 20.5	Graphite	1150	70	2.2/0.8	23
71	111 s.i.	10.0	60.1	278.5	none	BN	1150	60	0.75	26
72	111 p	7.5	45.76	199.7	GaTe 17.3	Graphite	1146	80	1.7/2.1	24
73	111 p	7.5	45.2	227.3	GaTe 53.5	Graphite	1148	70	1.7/1.7	22
74	111 p	7.5	45.1	212.2	Zn 53.6	Graphite	1150	35	1.7	24
75	111 p	7.5	45.1	212.1	Zn 53.6	Graphite	1150	35	1.7	14.8
					GaTe 53.3			35	1.7	7
76	111 n	7.5	45.33	210.7	GaTe 14.9	Graphite	1150	35	1.7	16
					Zn_3P_2 75.6			35	0.76	11.3
77	111 p	7.5	45.89	221.04	Zn 165	Graphite	1150	35	0.76	15.6
		7.5	45.12	220.1	TE 10.6			35	2.1	8.7

TABLE I (continued)

GALLIUM ALUMINUM PHOSPHIDE

GLPE	Substrate	Ga (gm)	Al (mg)	Ambient or Dopant	Dopant (mg)	Container	Growth Temp. °C	Temp. Span °C	Growth Rate °C/min	Thickness (microns)
78	111 p	7.5	45.16	NH_3	Zn 80	Graphite	1150	30	0.76	13.2
		7.5	44.55	NH_3	Te 11.5			35	2.1	9.1
79	111 n	7.5	44.05	NH_3	Te 11	Graphite	1150	41	1.7	17.4
		7.5	45.84	NH_3	none			40	1.7	13.1
80	111 p	7.5	45.03	NH_3	Zn 115	Graphite	1150	39	1.7	13.1
		7.5	45.2	NH_3	Te 10.1			40	1.7	7.8
81	111 p	7.5	45.2	NH_3	Zn 116.8	Graphite	1150	34	0.76	15.6
		7.5	45.2	NH_3	Te 10.1			34	1.7	10.4
82	111 n	7.5	44.6		Te 10.8	Graphite	1150	30	1.7	13.9
		7.5	44.8		Mg 27.1			35	0.76	10.4
83	111 p	7.5	45.3	NH_3	Zn 208	Graphite	1150	35	0.76	15.7
		7.5	45.3	NH_3	Te 11.7			45	1.7	8.7
84	111 n	7.5	45.4	NH_3	Te 10.9	Graphite	1150	45	1.7	17.4
		7.5	45.5	NH_3	Mg 1.16			35	1.7	5.2
85	111 p	7.5	45.5	NH_3	none	Graphite	1150	60	1.7 ∿ 50	25
86	111 p	7.5	44.8	NH_3	Zn 200	Graphite	1150	35	0.76	14
		7.5	44.6	NH_3	none			40	2.1	10.4
87	111 p	7.5	44.2	NH_3	Zn 232	Graphite	1150	35	0.76	23.4
		7.5	44.7	NH_3	Te 10.9			30	2.1	11.8
88	111 p	7.5	44.3	Ge	Zn 200	Graphite	1150	35	1.7	14.7
		7.5	44.3	Ge	Te 11.4			35	1.7	10.1
89	111 p	7.5	45.0	B	Zn 104	Graphite	1150	35	0.76	15.2
		7.5	45.2	B	Te 10.4			30	1.7	12.1
90	111 p	7.5	44.9	Sb	Zn 112	Graphite	1150	35	1.7	14.3
		7.5	44.9	Sb	Te 10.8			35	1.7	11.8

TABLE II

Gallium Aluminum Phosphide

Composition Analysis of Aluminum in $Ga_{1-x}Al_xP$

Sample	Cross Section	Surface
GLPE-1	0.78 – 0.74	0.91 – 0.92
-3	0.86 – 0.81	0.90 – 0.91
-4	0.82 – 0.78	0.89 – 0.91
-5	0.86 – 0.83	0.87 – 0.91
-6	0.90 – 0.88	0.90 – 0.91
-7	0.83 – 0.79	0.89 – 0.91
-10	0.75 – 0.67	0.72
-11	0.87 – 0.81	0.86
-14	0.86 – 0.82	0.80 – 0.83
-15	0.82 – 0.78	
-16	0.83 – 0.77	0.81
-17	0.64 – 0.61	0.04 – 0.10
-18	0.80 – 0.72	0.89
-19	0.83 – 0.82	0.83 – 0.82
-20	0.83 – 0.82	0.83 – 0.82
-21	0.65 – 0.50	0.49
-22	0.43 – 0.30	0.30 – 0.34
-24	0.42 – 0.30	0.38
-25	0.74 – 0.67	0.72

TABLE II (continued)

Gallium Aluminum Phosphide

Composition Analysis of Aluminum in $Ga_{1-x}Al_xP$

| Sample	Cross-Section	Surface	
GLPE – 26	0.74 – 0.65	0.74 – 0.73	
27	0.77 – 0.65	0.73	
28	0.77 – 0.74	0.74	(0.74)
29	0.75 – 0.65	0.65	(0.65)
30	0.76 – 0.72	0.61	
31	0.78 – 0.70	0.69	(0.75)
32	0.78 – 0.71	0.73	
33	0.77 – 0.74	0.73	
34	0.77 – 0.75	0.74	
35	0.78 – 0.74	0.76	
36	0.78 – 0.73	0.74	
37	0.78 – 0.75	0.75	
38	0.78 – 0.76	0.75	
39	0.77 – 0.76	0.76	(0.75)
40	0.78 – 0.75	0.72	
41	0.77 – 0.75	0.74	(0.76)
42	0.74 – 0.71		(0.74)
43	0.74 – 0.73		(0.76)
44	0.75 – 0.72	0.72	(0.75)
45	0.73 – 0.68	0.72	(0.73)
46	0.73 – 0.69		
48	0.77 – 0.74		
49	0.78 – 0.75		(0.74)
50	0.78 – 0.74		(0.75)
51	0.78 – 0.75	0.75	(0.74)
52	0.78 – 0.75	0.75	(0.75)
53	0.77 – 0.74	0.56	
54		0.73	
55	0.54 – 0.46	0.46	
57		0.75	
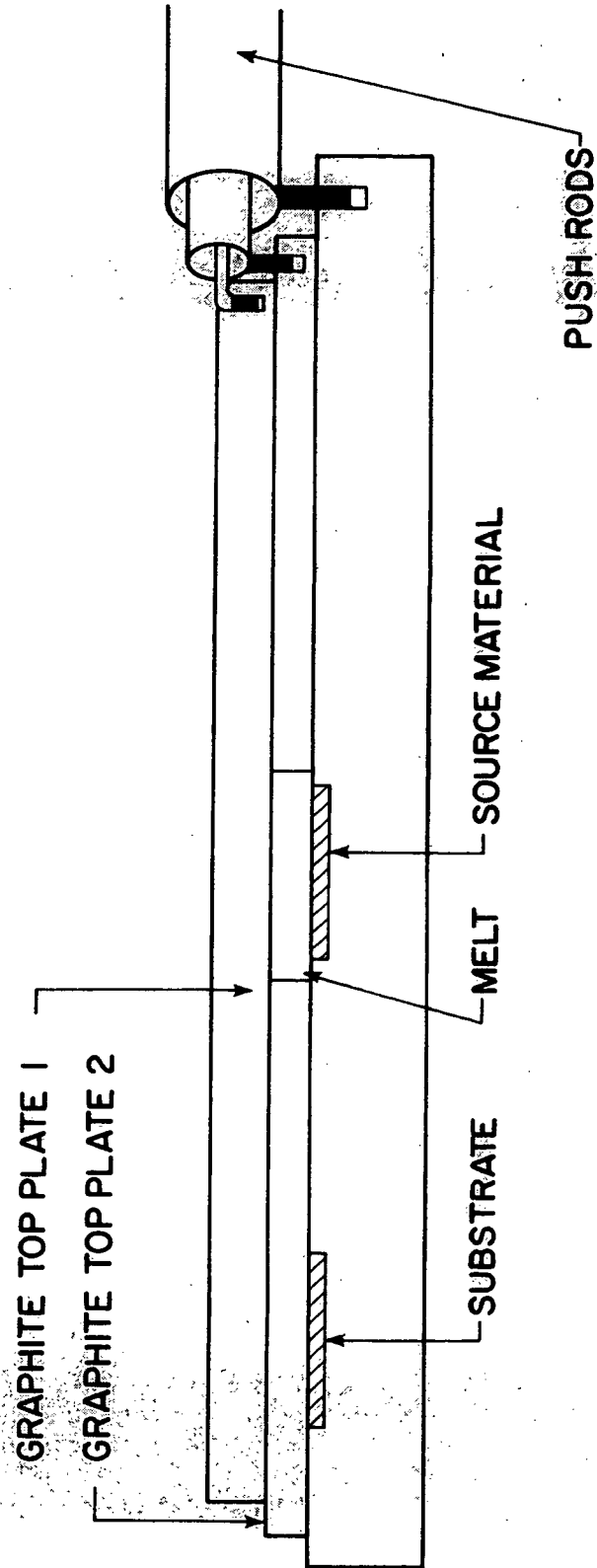
Figure 1
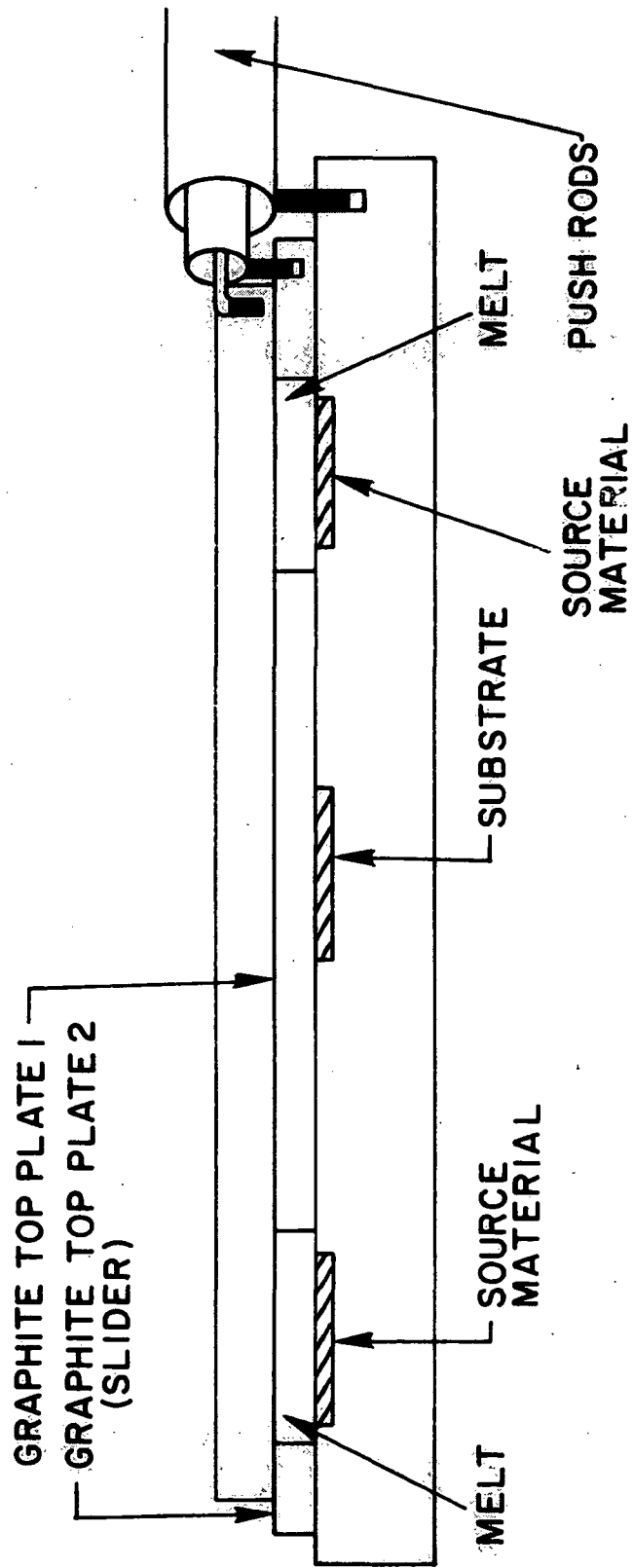
FIGURE 2

Figure 3

Figure 4

$Ga_{1-x}Al_xP$
GROWTH TEMPERATURE, 1150°C

mg-Al/gm-Ga

$X \ (Ga_{1-x}Al_xP)$
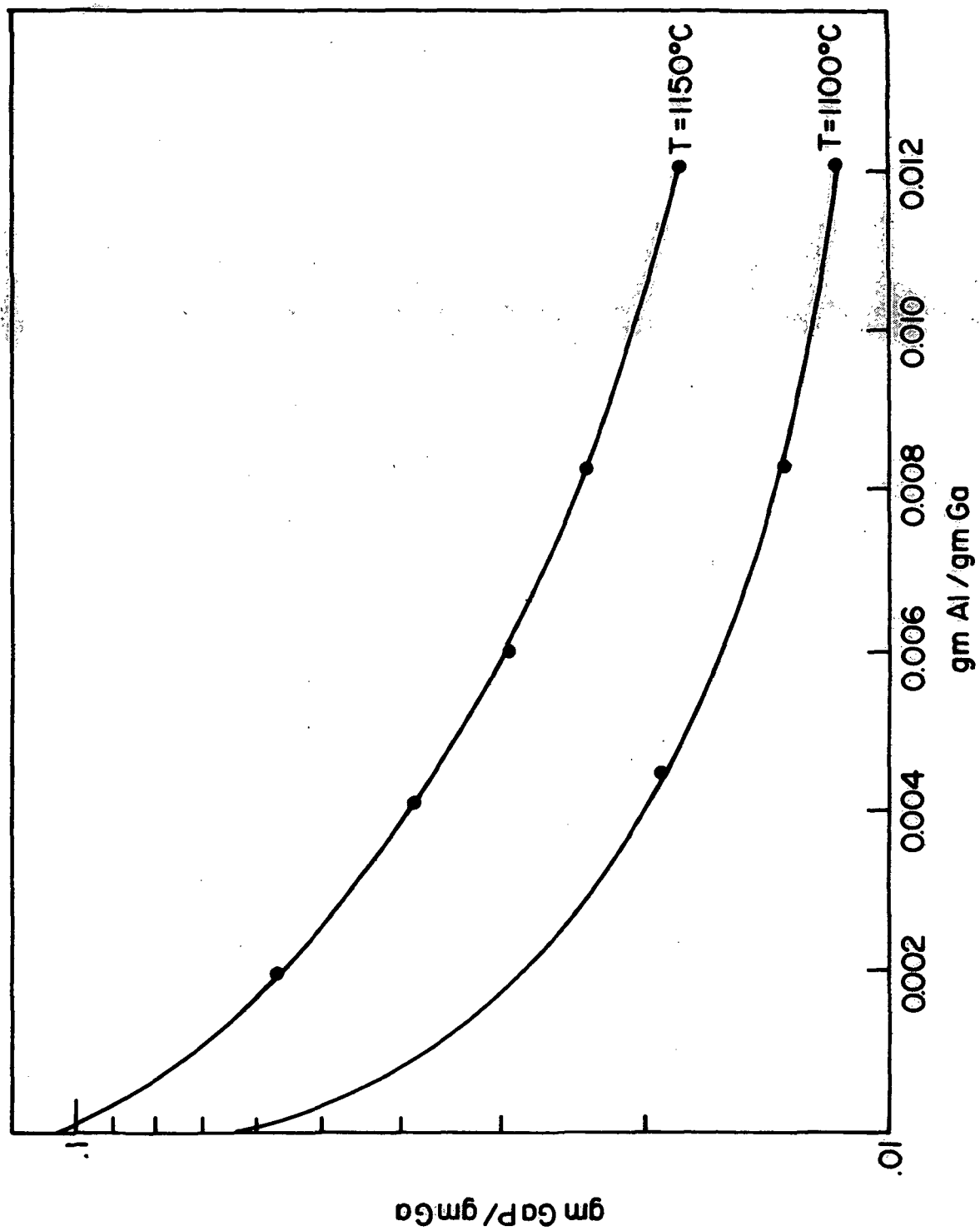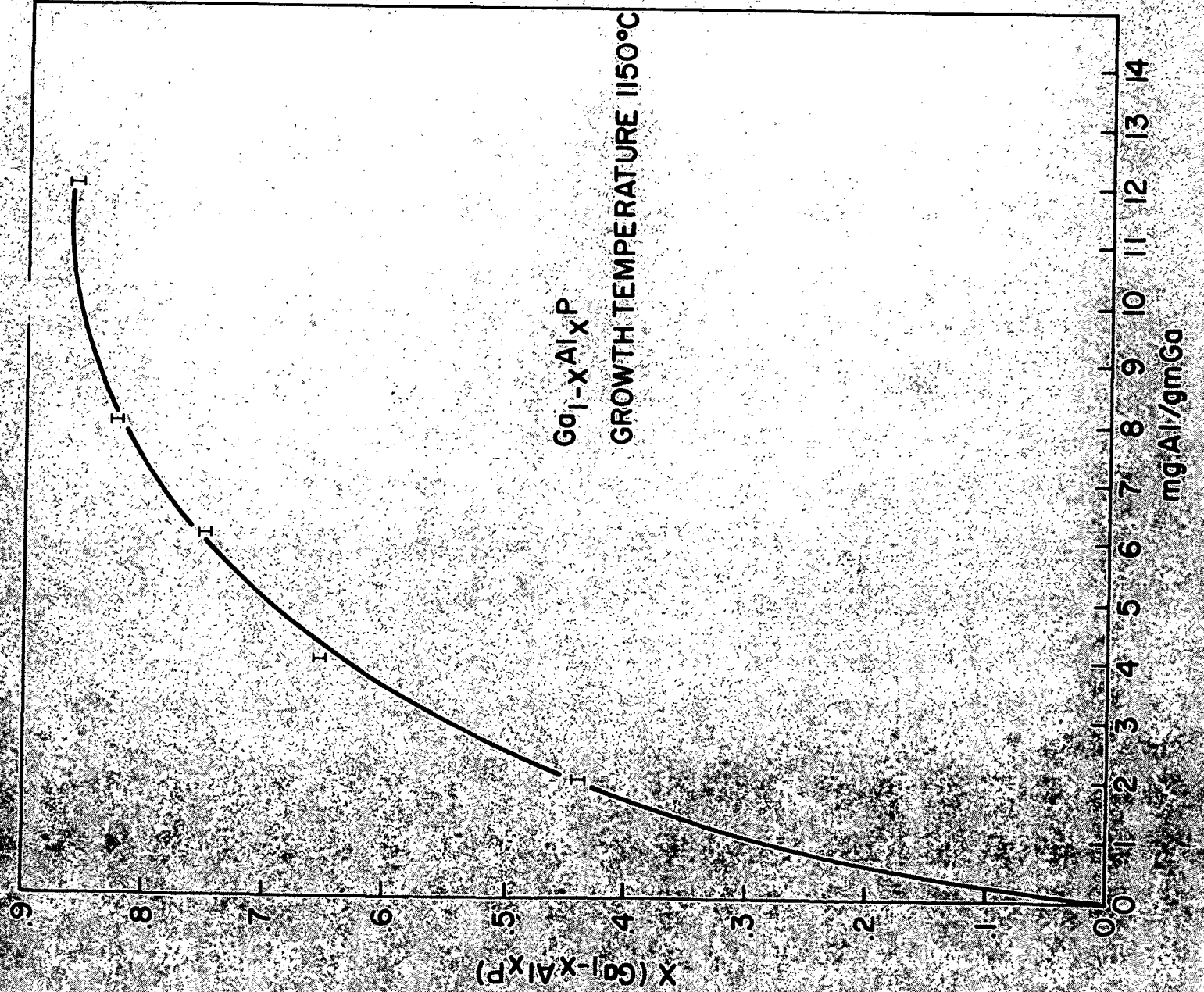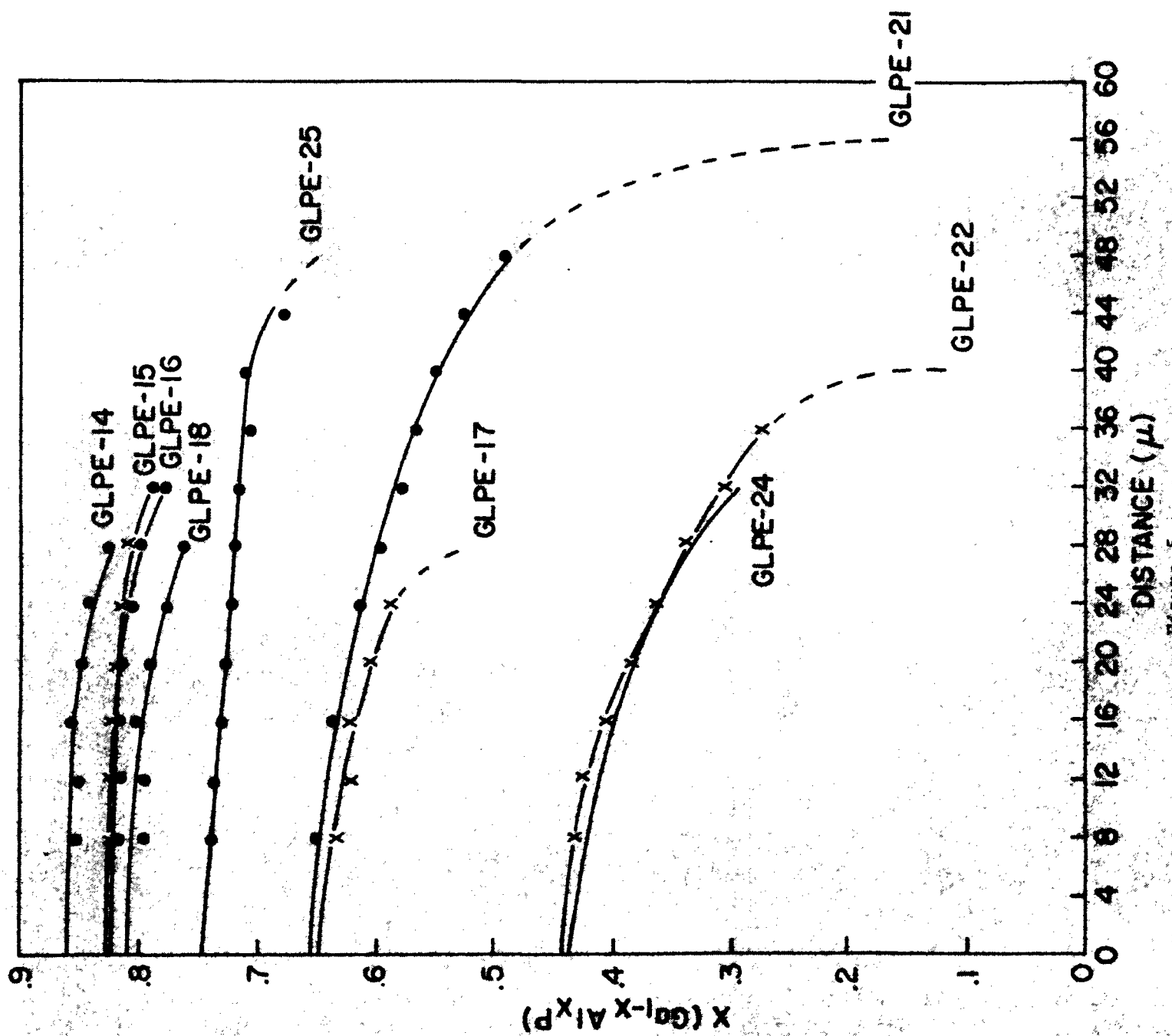
Figure 5

PHYSICAL PROPERTIES

Electrical Measurements.- Hall measurements of the electrical properties
were made on single crystal samples which were in the form of ultrasonically
cut spiders. Electrical contact was made by alloying ohmic contacts to the
samples. A compilation of these electrical measurements is shown in Table III.
The Hall effect measurements were made at both 300°K and 77°K on epitaxial
layers grown either on semi-insulating GaP substrates or on substrates of the
opposite conductivity type. Only those electrical properties which could be
reproducibly measured several times are reported.

The electrical measurements have been grouped into three catagories: un-
doped samples, tellurium doped samples and zinc doped samples and the major
differences which characterize each of these catagories is presented.

Undoped Samples - From Table III, the background impurity level measured
on a sample with no aluminum added (GaP - sample 47) is $4 \times 10^{16}/cm^3$ "n"
type. This is within the ordinary range for nominally undoped GaP. However,
epilayers of (GaAl)P grown either in the boron nitride apparatus (samples 43,
49, 50, 51) or in the graphite apparatus (samples 52, 57, 58) are typically
$2-5 \times 10^{18}/cm^3$ "p" type. No significant carrier freeze-out occurs at 77°K and
this would indicate that the acceptor state is probably a relatively shallow
level.

Thus, the addition of aluminum to undoped GaP changes the types and the
background carrier concentration (see sample 55 also with $x \simeq .50$) and this
background level is independent of the growth apparatus used. Possible reasons
for this comparatively high background acceptor concentration are not readily
apparent. The background p doping level decreases as the growth rate is in-
creased (sample 53). This sample was grown at twice the normal rate of growth
and is "p" type with 1×10^{18} cm^3 carriers.

Tellurium Doped Samples - Intentionally doped epitaxial layers were pre-
pared by adding the dopant to the melt during load-up of the growth apparatus.
Although several impurities were used, the principal dopants investigated were
tellurium and zinc.

Epilayers were grown from a series of melts variously doped with tellurium
to establish the amount of tellurium necessary to compensate the background
"p" level and to determine the effects of this doping on the electrical
properties of the alloy. Samples 35, 45 and 33 were prepared from melts con-
taining 1 mg ($5 \times 10^{18}/cm^3$), 11 mg ($5 \times 10^{19}/cm^3$) and 101 mg ($5 \times 10^{20}/cm^3$),
respectively. The lowest level of tellurium in the melt necessary to com-
pensate the background level was $5 \times 10^{19}/cm^3$ at a cooling rate of $\sim .75°C/min$
and this gave a carrier concentration of $5.2 \times 10^{16}/cm^3$ "n" type in the alloy.

The incorporation of tellurium in the alloy is enhanced and can be changed
by 3 orders of magnitude by increased growth rates. A series of tellurium
doped epilayers (samples 34, 45, 61, 62) were grown at different cooling rates
and the corresponding carrier concentrations were measured. The initial

tellurium concentration in the liquid for each run was approximately 10 mg and this corresponds to the approximately 5×10^{19} atoms/cm^3 that was necessary to compensate the p-type background impurity level at the standard cooling rate of 0.76°C/min. The cooling rates used were 0.76, 2.0, ∿ 10, and ∿ 50 °C/min and the corresponding carrier concentrations in the alloys were 5.2×10^{16}, 5.4×10^{17}, 3.6×10^{18} and 6.6×10^{19} per cm^3.

Zinc Doped Samples – Several epilayers were grown with various amounts of zinc added to the melt (samples 39, 40, 41, 44). Due to the high undoped background "p" level, the effects of the zinc doping were inconclusive. The only noticeable effects the zinc incorporation had on the electrical properties of the epilayer were that the carrier mobilities at both 300°K and 77°K were higher and that there was more than a factor of 10 increase in the carrier freeze-out as compared to the undoped "p" samples.

TABLE III

Electrical Measurements on $Ga_{1-x}Al_xP$ with $x \simeq 0.75$

GLPE	Dopant	Type	ρ	300°K R_H	μ	n	ρ	77°K R_H	μ	n
30	Sulfur	n	0.013	0.26	20	2.3×10^{19}				
31	Sulfur	n	0.022	0.40	18	1.5×10^{19}	0.034	0.84	24	7.4×10^{18}
33	Tellurium	n	0.034	1.09	31	5.7×10^{18}	0.068	1.0	15	6.1×10^{18}
34	Tellurium	n	0.10	1.69	18	3.6×10^{18}				
39	Zinc	p	0.10	3.69	38	1.8×10^{18}	2.84	263	93	2.4×10^{16}
43	Undoped	p	0.078	1.19	15	5.2×10^{18}	1.35	13.2	9	4.7×10^{17}
44	Zinc	p	0.088	2.02	23	3×10^{18}	3.84	169	44	3.7×10^{16}
45	Tellurium	n	6.79	17.6	18	5.2×10^{16}	43.1	3.4	3	4.2×10^{15}
*47	Undoped	n	1.14	160	137	4×10^{16}	1849	1.2×10^6	655	5.2×10^{12}
48n	Undoped	n	2.12	358	179	1.7×10^{16}	37.7	2586	607	2.7×10^{14}
48p		p	0.089	1.70	19	3.7×10^{18}	3.79		11	1.6×10^{17}
49	Undoped	p	0.135	2.4	18	2.6×10^{18}	7.16	106	14	6.2×10^{16}
50	Undoped	p	0.168	2.2	13	2.8×10^{18}				
51	Undoped	p	0.146	3.66	24	2.7×10^{18}	6.46	65.1	10	9.6×10^{16}
52	Undoped	p	0.168				7.72	8.09	11	7.7×10^{16}
53n	Undoped	n	0.56	93.3	166	6.7×10^{16}	20.4	4926	826	1.3×10^{15}
53p		p	0.289	5.52	19	1.1×10^{18}	17.6	1414	79	4.7×10^{15}
54n	Undoped	n	5.72	736	128	8.5×10^{15}	23.1	8085	315	7.7×10^{14}
54p		p	0.07	1.17	16	5.3×10^{18}	1.75	9.26	5	6.7×10^{17}
55	Undoped	p	0.35	6.81	23	9.1×10^{17}	20.2	1052	57	5.9×10^{15}
57	Undoped	p	0.123	2.02	16	3.1×10^{18}	5.39	40.1	7	1.5×10^{17}
58	Undoped	p	0.121	1.80	15	3.5×10^{18}	4.87	31.2	6	2.0×10^{17}
59	Silicon	p	0.270	3.15	12	1.9×10^{18}	8.0	42.1	5	1.6×10^{17}
61	Tellurium	n	0.0022	0.095	42	6.6×10^{19}	0.0019	0.094	48	6.6×10^{19}
62	Tellurium	n	0.372	11.8	31	5.4×10^{17}	4.56	20.2	4	3.1×10^{17}

*GLPE-47 is a GaP epilayer grown from a BN holder to determine background impurity level.

GLPE-55 has a lower aluminum concentration (x = 0.5).

Optical Absorption.- Optical absorption measurements were taken at 6°K by the usual methods using a Cary Model 14 spectrophotometer equipped with a low temperature cell. The epitaxial layers were thick enough so that the substrate could be lapped off and both surfaces of the layer could be polished. These thinned samples could be measured without additional support. Absorption coefficients were calculated using the equation:

$$\alpha = \frac{(1-R)^2 e^{-\alpha x}}{1-R^2 e^{-2\alpha x}}$$

using for R a value of 0.28. The results are plotted as the square root of the absorption coefficient versus photon energy in Figs. 6 and 7. We have also included data on GaP and AlP.

The energy gaps of GaP and AlP are 2.338 and 2.53 eV respectively. For indirect band gap materials, $\alpha^{1/2}$ should depend linearly on $h\nu$. Thus, by extrapolating the range of $\alpha^{1/2}$ between 12 and 5 $cm^{-1/2}$ toward $\alpha \to 0$, we define E_g in the alloys using the known end points as anchors. We discount the low α deviations since the data on our thin samples is least reliable in the low absorption regime. The composition of each of these samples was measured by electron microprobe. The energy gap as a function of alloy composition is plotted in Fig. 8. The length of the bar indicates the cross sectional variation in the measured composition. The data clearly indicates that E_g is not a linear function of composition. This is rather surprising since the $Ga_{1-x}Al_xP$ system because of its complete lattice match might have been expected to be more ideal.
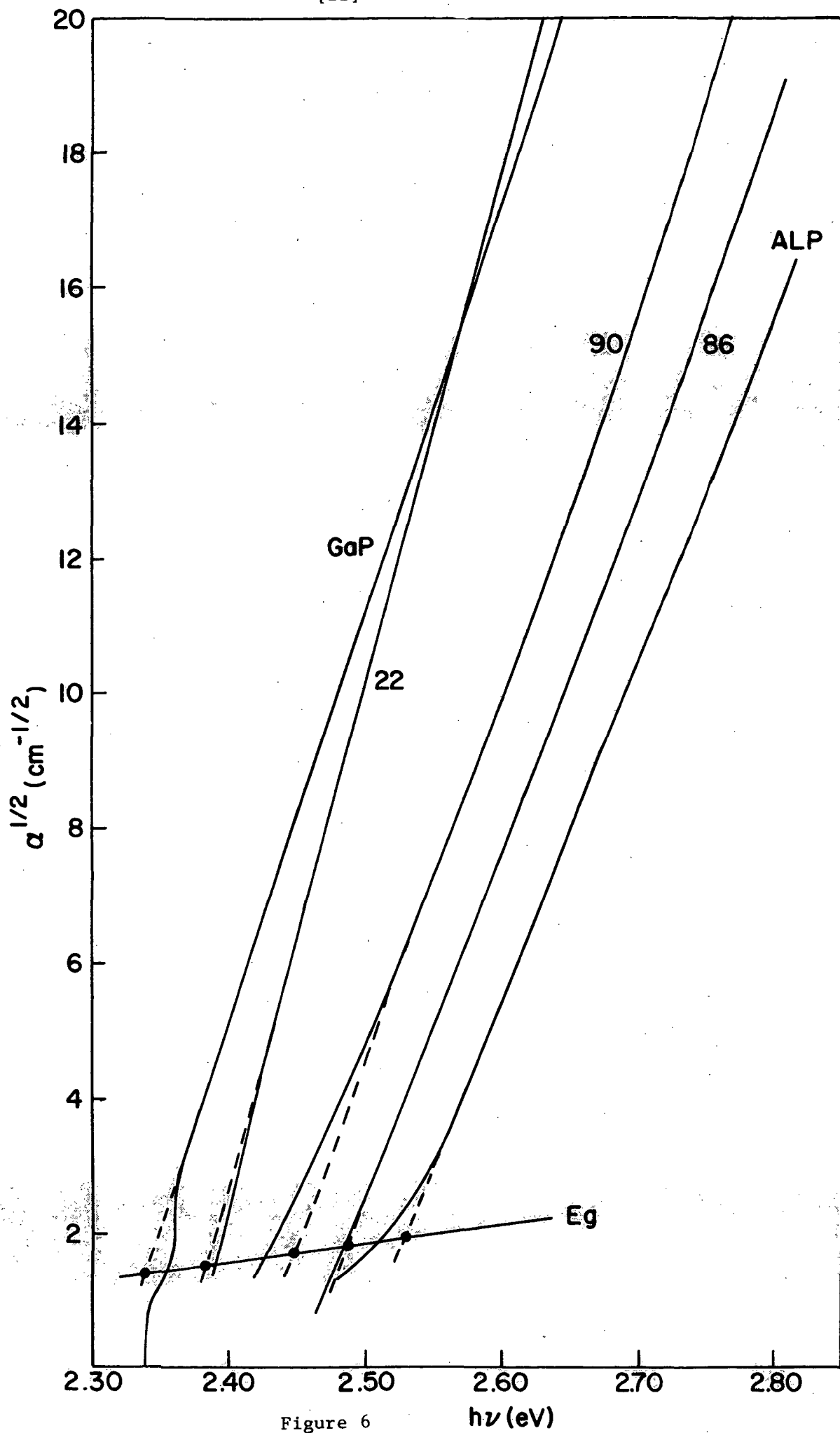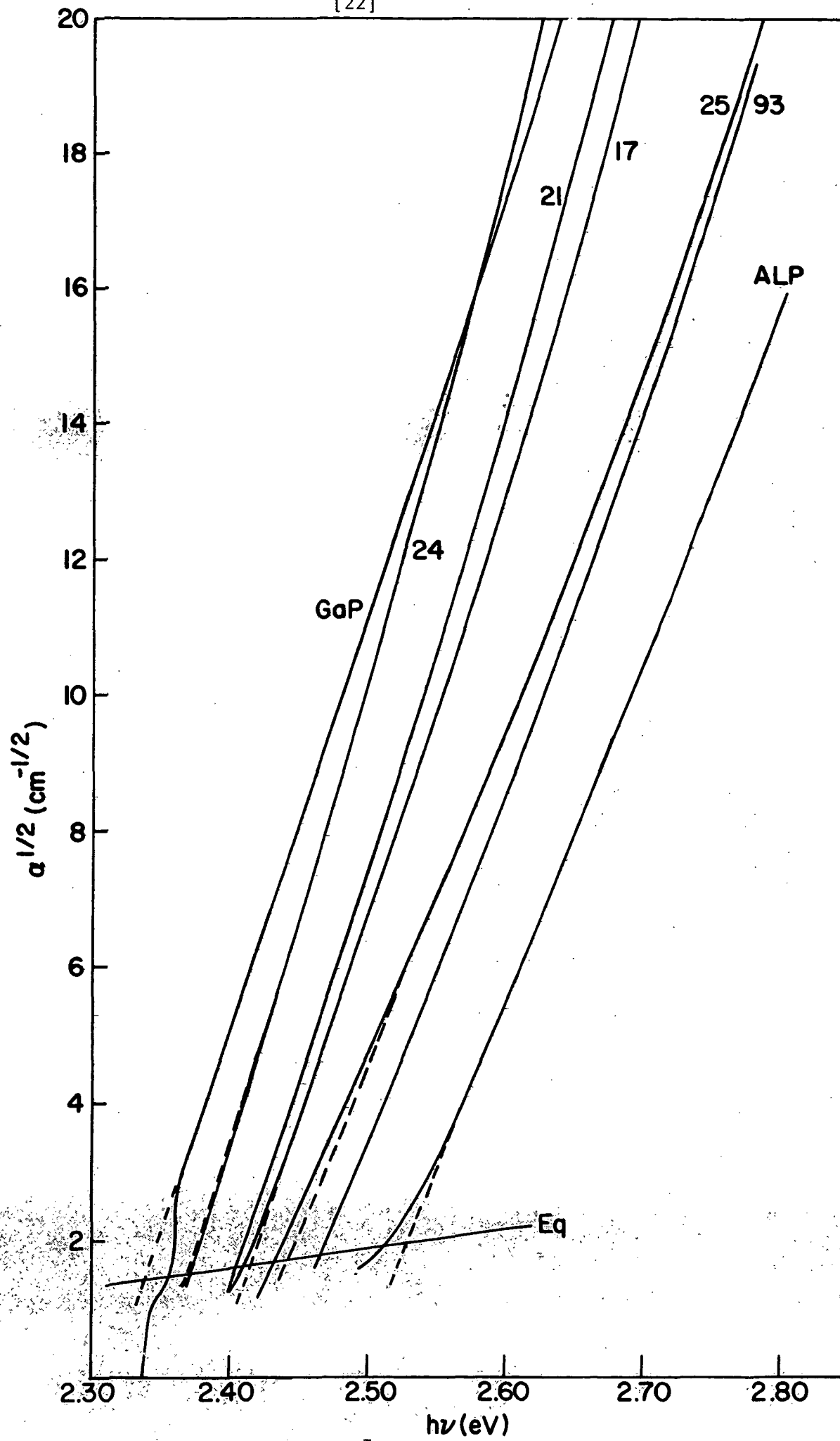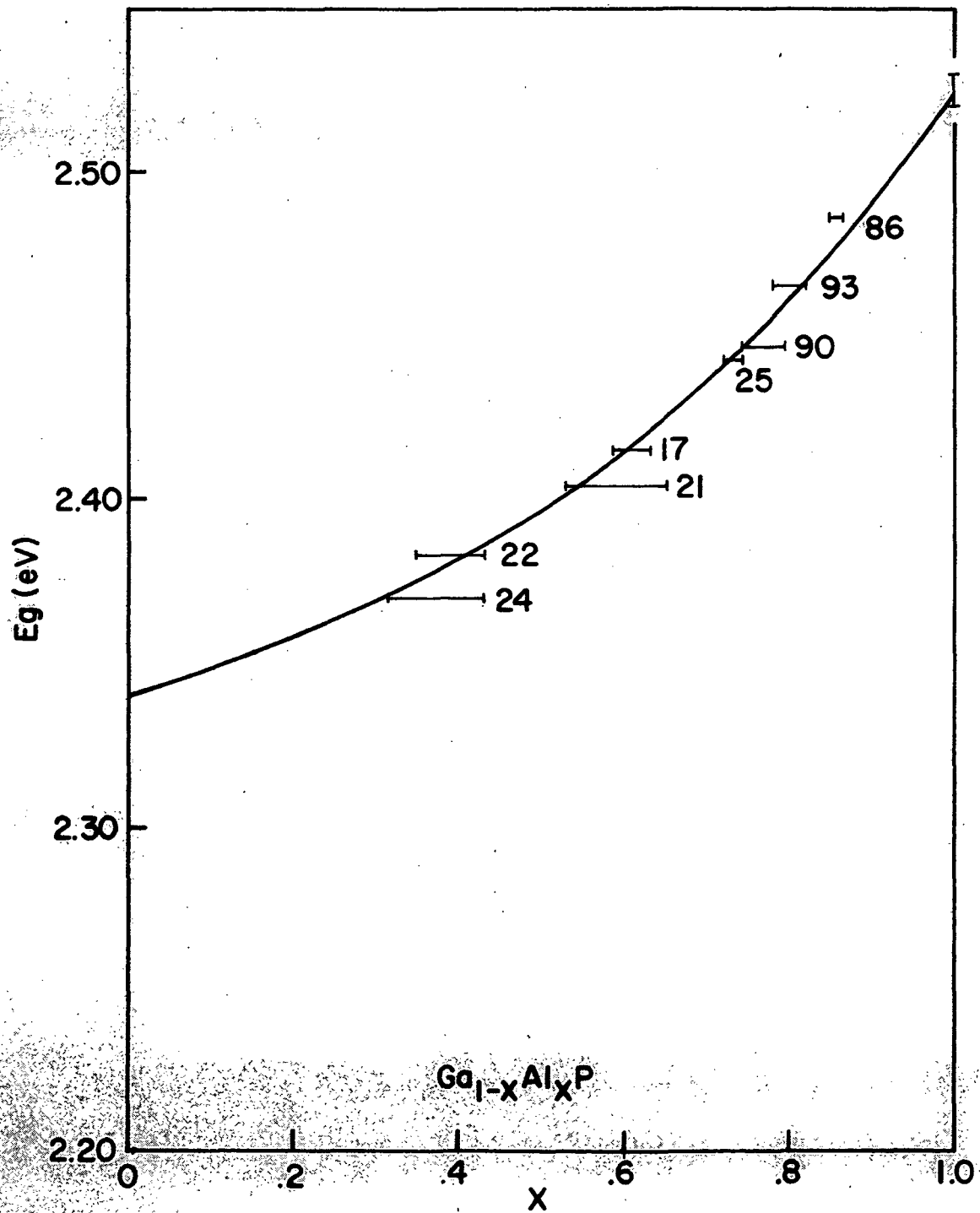
Figure 6

Figure 7

Figure 8

Photoluminescence Measurements.- Photoluminescence measurements have been
made on most of the (GaAl)P epilayers. The data were taken at 2°K and in some
cases at 77°K when the temperature dependence of the spectra seemed of im-
portance. Because of the high band gap of (GaAl)P at 2°K (> 2.43 eV), efficient
excitation could only be achieved using a high pressure Hg lamp with suitable
filtering to isolate the 3-4 eV region of the lamp's output. Even with the high
absorption obtained with this excitation mode, penetration of the UV was
sufficient to excite the GaP substrate in most samples. However, this substrate
luminescence is readily identifiable in the data and can be ignored. It should
be noted that the photoluminescence measurements should emphasize the behavior
of the surface of the overgrowth as compared to the optical absorption measure-
ments.

The photoluminescence, with few exceptions, contains two bands, which
peak at 2.317 - 2.338 eV (Band I) and at 2.278 - 2.304 eV (Band II) respectively.
These bands appear to be present independent of any intentional doping. Figs. 9
10, and 11 show the 2°K luminescence of undoped, Zn doped and nitrogen doped epi
layers respectively. Bands I and II are always present and, except for 85
and 93, they are the dominant emission bands, although sample 95 has a more
intense peak at 2.42 eV and 2.37 eV. We assume that the spread in peak position
of band I of 0.021 eV is due to compositional variation. A similar argument
should hold for band II. The origin of these bands has not been determined,
but their resemblance to donor-acceptor pair bands in GaP suggests that this
pair emission is maintained in the alloy. In fact, using 84 as an example
(see Fig. 9) we find that the separation between the peak of band I and E_g is
0.117 eV. This agrees closely with the separation of 0.121 eV for the C-S
pair band in GaP. The C-S pair band is most commonly observed in undoped GaP
and this identification is tentatively assigned to band I in the alloys.

Let us now examine the individual luminescence plots. The undoped samples
shown in Fig. 9 and the nitrogen doped samples in Fig. 11 except for detail
appear very similar. They have emission bands at energies higher than band I.
At this point it appears that the luminescence observed in Figs. 9 and 11 arises
from unintentional doping. For both bands I and II (as well as for the higher
energy emission, which probably is due to nitrogen similar to GaP) the im-
purities responsible apparently are introduced during the normal growth process.

On the other hand, the broad band between 2.1 and 2.2 eV in the Zn doped
samples is only seen with Zn present and is either a pair band or a complex
such as Zn-O on nearest neighbor sites. To test the hypotheses that Zn-O
complexes exist in the (GaAl)P alloys we have heat treated two parts of a Zn-doped
sample at 1000°C and quenched these samples. One sample was annealed at 600°C
for 4 hours. The quenched sample lost most of the $\sim$ 2.1 eV peak as would be
expected if it is due to the Zn-O complex. However, the complex was not re-
formed on annealing and this leaves us without a completely satisfactory ex-
planation.

Various amounts of tellurium were added as a dopant in several other over-
growths (samples 28, 29, 33, 34, 35, 45, 46, 60, 61). At sufficient tellurium
levels to convert the undoped p type material to n type, a new emission band
emerged which varied in peak position from 2.17 eV to 2.22 eV with increasing

amounts of tellurium and had a half-width of 150 meV. This is shown in Fig. 12 where the spectra for samples with 1, 10, 101 mg tellurium added are shown bottom to top respectively (vertical scale arbitrarily displaced for clarity). The corresponding carrier concentrations are: 1 mg = 2.6×10^{18} cm^{-3} p type; 10 mg = 5×10^{17} cm^{-3} n type; 101 mg = 5.7×10^{18} cm^{-3} n type.

As discussed in the section on absorption measurements, the variation of E_g with composition as determined by optical absorption deviates considerably from linearity. We have also measured the photoluminescence spectra of many "undoped" overgrowths and find that they exhibit the characteristic two band green luminescence, previously labelled band I and band II. Figure 13 shows the peak of band I vs the electron microprobe determined alloy composition. We also show the band gap curve from absorption measurements presented earlier in the report. As can be seen, the degree of non-linearity is similar in P.L. to that in absorption if the P.L. curve is extrapolated to 2.213 eV, which is the peak energy of the C-S pair band in GaP. This level is the dominant emission band in GaP grown in the present apparatus. The separation between E_g and the P.L. curve in GaP is 125 meV, while at the AlP end it is 145 meV. This could be explained by either or both donor and acceptor binding energies increasing as the Al concentration increases. On the other hand, the peak of the C-Si pair band emission in GaP occurs at 2.195 eV, which would give an almost identical bowing to the P.L. curves as the E_g curve. However, we have not been able to definitely verify whether either set of donor-acceptor pairs is responsible for this luminescence.

Thus, we have correlated the normal photoluminescence peak energies with alloy composition and shown that they have the same dependence as E_g. This data clearly indicates a non-linear composition dependence of the photoluminescence peak energy similar to that observed for the absorption edge.
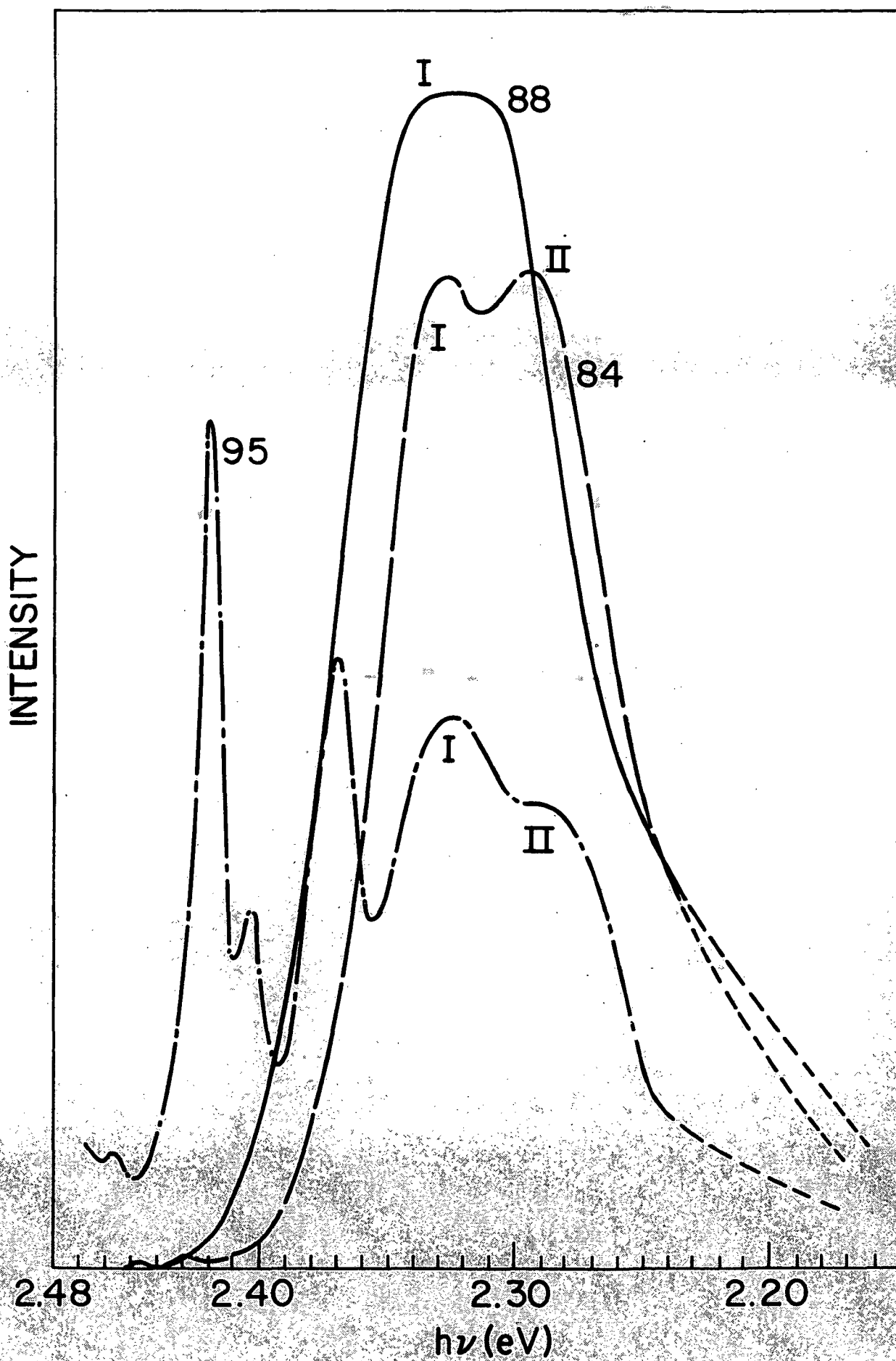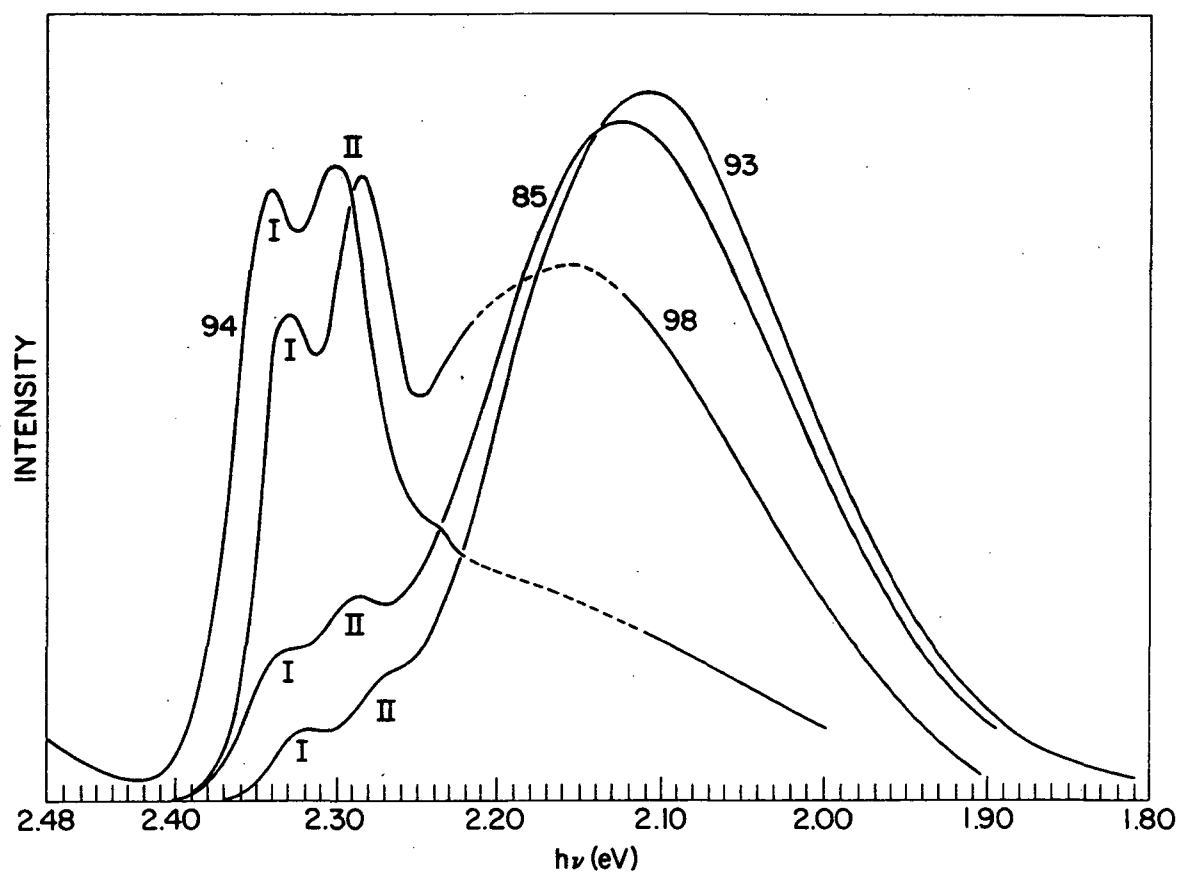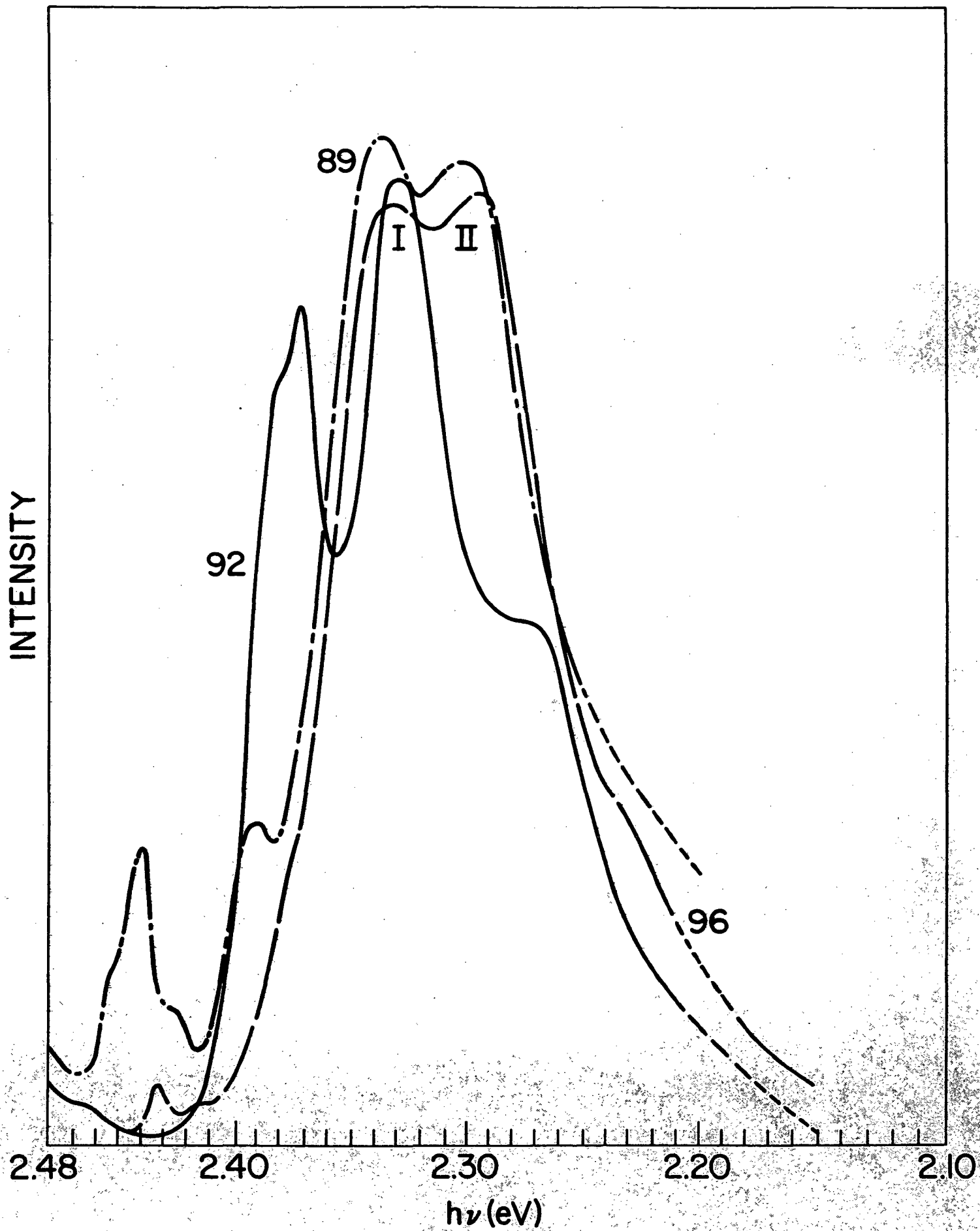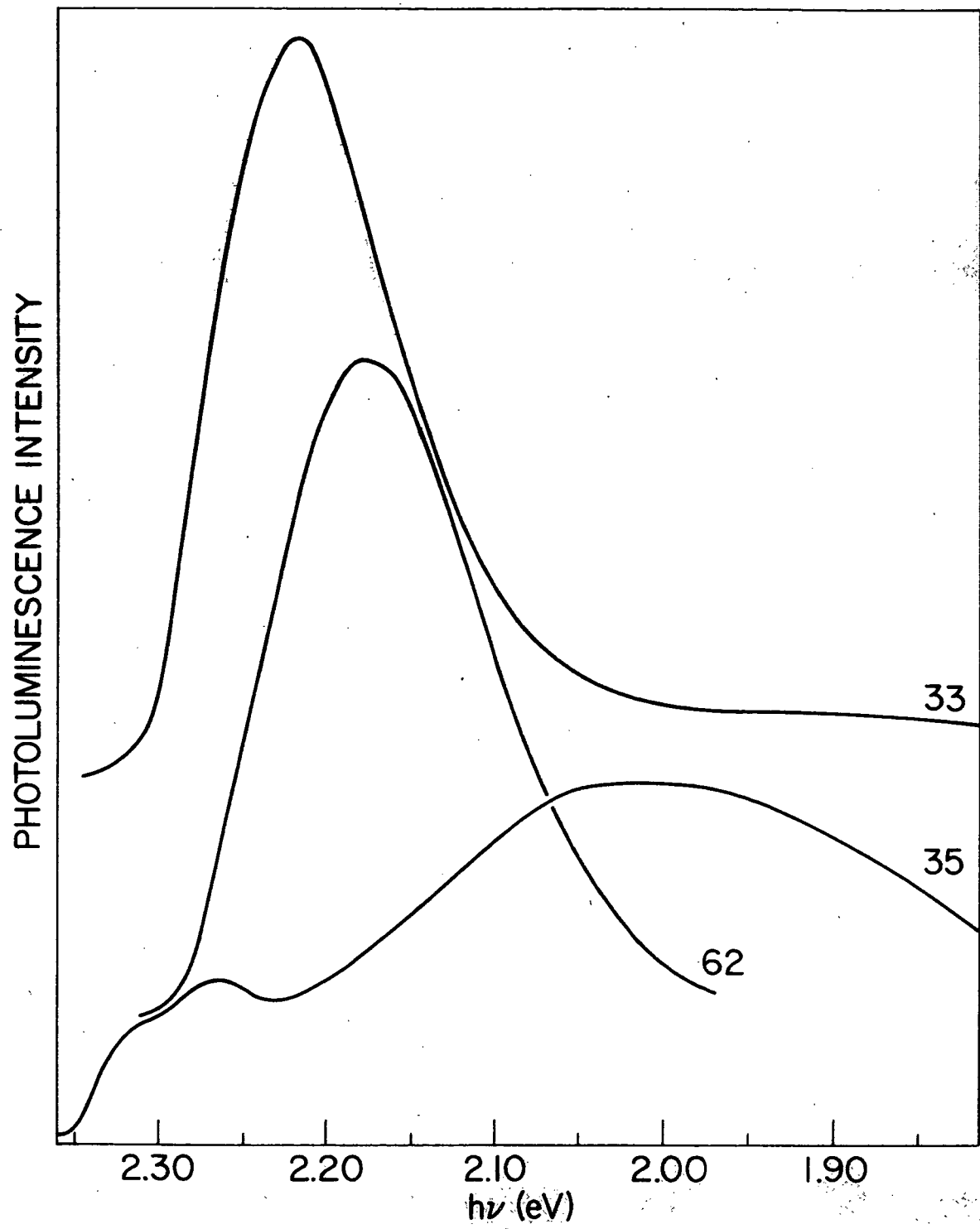
Figure 9

Figure 10
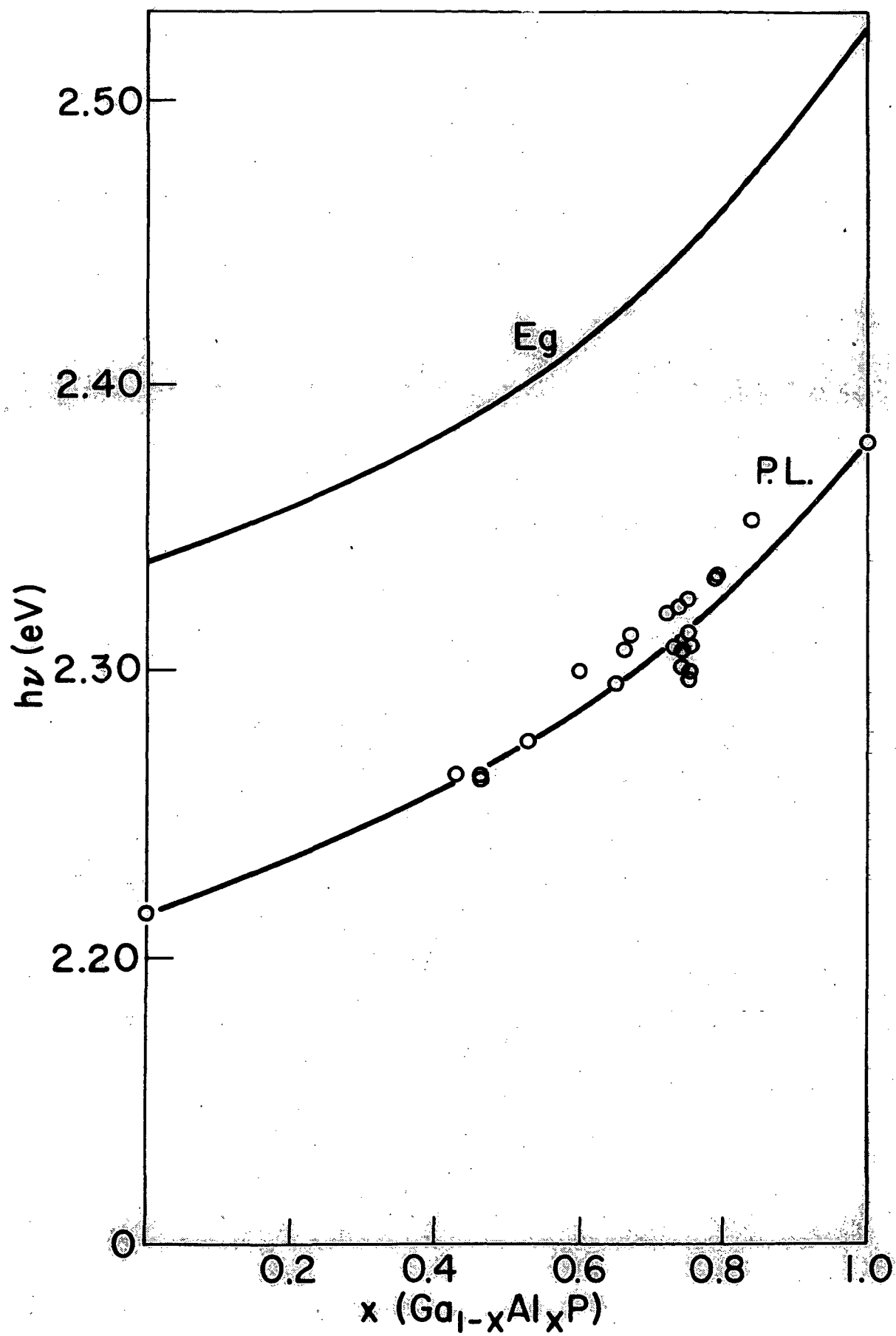
Figure 11

Figure 12

Figure 13

FABRICATION AND MEASUREMENTS OF p-n JUNCTION DIODES

The overgrowths were made using the "push-pull" technique previously described and which has provisions for maintaining two independently doped melts between which the sample is moved to grow the p- and n-layers (Fig. 2). The GaP source wafers and a (111) oriented, p-type GaP substrate are maintained in recesses cut in the lower plate. The Ga-Al melt with the intentionally added donor and acceptor impurities are contained in the wells in the slider plate. A typical composition of the n-type solution is 7.5 gm Ga, 45 mg Al, 350 mg GaP source wafer and 10 mg Te (for the p-solution approximately 100 mg Zn is substituted). An inert Argon ambient is maintained during the growth cycle, and there are provisions in the flow apparatus for incorporating other gases (e.g. NH_3). For the nitrogen doped samples, 1% NH_3 in Ar mixture was used which could be diluted with additional Argon. The n and p layers are grown by alternately contacting the substrate with the n and p solution during the cooling cycle. The p-layer (about 15 microns thick) is produced by slow cooling the solution from 1150°C to 1120°C. The n-layer (about 10 microns thick) is grown by slow cooling from 1120°C to 1080°C. Typical cooling rates were approximately 0.75°C/min. A few overgrowths were made with the p and n epilayers reversed, in which case an n-type substrate was used. There was apparently no significant difference in the p on n and n on p junctions.

Microscopic examinations of the overgrowths were made on sections cleaved on a (110) plane at 90° to the crystal surface. The cleaved surfaces were etched with a solution of $HF:H_2O_2:H_2O/1:20:100$. By illumination of this cleavage plane with light at normal incidence, the etched junction could generally be seen. The junctions with few exceptions were very planar and the epitaxial layers showed good perfection.

For the formation of electroluminescent diodes, the substrate side of the wafer was thinned to reduce the series resistance and the crystal was cleaved into small triangular platelets less than 1 mm on an edge. Ohmic contacts to the crystal were made by simultaneously alloying either Au-Sn or Au-In eutectic and Au-Zn (96%-4%) dots to the n and p sides, respectively, of the cleaved sections. The platelets were mounted on a standard TO-5 header. The junction area was generally about 2×10^{-3} cm^2.

Electrical Properties.- The electrical properties of a number of variously doped diodes were studied. The current-voltage characteristics of all diodes had the same general behavior. This is shown in Fig. 14 for a typical diode containing Zn on the p side and Te on the n-side. Over a current range of several decades, the current varied exponentially with voltage as $\exp(eV/\beta kT)$ with $\beta \sim 2$. Such values of β usually indicate that recombination in the space charge region predominates. The bending over of the curve at higher current levels is due to the rather high series resistance of the device. This high resistance is probably related to the rather low mobility which we have measured in similarly doped samples of these (Ga,Al)P alloys. Also, excess currents are usually found at low currents as manifested by the deviation from the exponential dependence.

These current-voltage curves are rather different from those reported for GaP, particularly in that the currents are substantially ($\sim \times 100$) lower at similar voltages (but also in that β is generally closer to the value 2). These features are not strongly dependent on the amount of dopant used.

Capacitance-voltage measurements were made on some of the better diodes. Figure 15 shows a typical C-V curve for a Zn and Te doped diode at 300°K. It can be seen that the square of the recriprocal capacitance per unit area is a linear function of the applied voltage. This dependence is characteristic of abrupt junctions. Extrapolation of the curve to zero reciprocal capacitance gives a "built-in-voltage" of 3.1 volts at 300°K. Such excess "built-in-voltages" can be caused by the presence of an i layer. The impurity concentration for the more lightly doped side (n-layer) derived from Table 3 is 6.7 x 10^{17} cm^{-3} and this value agrees quite well with the value of 8.3 x 10^{17} cm^{-3} as measured on the same sample by the Hall technique. All the diodes measured showed C-V curves characteristic of abrupt junctions except for the more heavily doped (n > 4 x 10^{18}) junctions.

Thus, the electrical properties of these diodes were demonstrated to be under control and their characteristics were generally similar to those observed with GaP diodes. However, no explanation is at hand for the substantially lower forward currents compared to GaP diodes and it should be noted that the diode series resistance is apparently rather high.

Optical Properties.- Electroluminescence spectra were measured for diodes fabricated from epilayers grown under various doping conditions. For spectral measurements, the diodes were focused on the entrance slit of a Bausch and Lomb grating monochromator, which has a resolution limit of 3 Å. An RCA 7265 or a Dumond 6911 photomultiplier (with S-20 and S-1 spectral characteristics, respectively) was used as a detector.

Comparison between the emission spectra of three different types of diodes at 300°K is made in Fig. 16. The diodes were pulsed in the forward direction at 60 ma dc with a 10% duty cycle. Type 1, "undoped," was a p-type epilayer with a high ($\sim$ 2 x 10^{18} cm^{-3}) concentration of unidentified, unintentional background doping together with a Te doped n-type layer. Type 2, "Zn-Te doped" had the p side Zn doped and the n side Te doped. Type 3 was "Zn-Te doped" in a similar manner, but was grown in an ammonia ambient with the isoelectronic dopant nitrogen thereby also added.

A summary of the various overgrowths made is given in Table 4. The estimated net carrier concentration for both layers is also given. These values are estimated from the dopant level in the melt and the cooling rate used, where earlier results correlating these parameters with carrier concentrations determined by Hall and resistivity measurements are used.

The emission spectra observed for these three types of diodes were characteristic of the particular dopant combination (i.e., type) and were relatively insensitive to changes in the dopant concentrations within any one diode type. The emission spectra of the type 1 and type 2 diodes were similar and consisted of two high energy peaks near 2.20 eV and 2.31 eV (weaker), together with a very broad ($\Delta h\nu \sim 350$ meV) red luminescence band with its peak near 1.71 eV. However, the type 2 diodes (Te-Zn doped) emit about ten times as much higher frequency blue-green light as the type 1 diodes and the red component is relatively weaker. This red component for the Zn-Te doped samples saturates more rapidly at high current levels than the blue-green component.

The type 3 diode emission is quite different and is dominated by a single high energy band which peaks at 2.29 eV and has a full width at half intensity of ~ 175 meV. The deep red luminescence band is not observed. The high energy band is at least a factor of 10 more intense than the blue-green component of the Zn-Te doped samples grown with no nitrogen. Along with this increase in intensity, the high energy band is narrower than the peaks in type I and type II diodes.

External quantum efficiencies of the diodes were measured with an integrating sphere type of apparatus. The quoted efficiency values are differential quantum efficiencies taken from the region where the light intensity varies linearly with the current. No attempt was made to optimize the diode behavior (e.g. by epoxy doming) before the efficiency measurements were made.

At room temperature, the most efficient type 3 diodes fabricated had quantum efficiencies of 4×10^{-5} at a current of 20 ma (diode area ~ 2×10^{-3} cm^2). However, only three or four diodes had efficiencies this high, most of the thirty or so fabricated having efficiencies nearer 10^{-6}. Although the nitrogen doping was changed by varying the amount of NH$_3$ in the gas stream between .01 - 1%, the statistical sampling was not good enough to correlate the diode efficiency with the NH$_3$ doping. However, when the Zn doping was decreased by a factor of four, less efficient diodes were obtained. The quantum efficiencies of the type 1 and type 2 diodes were substantially less than the type 3 diodes and were not measurable. The brightness of the nitrogen doped type 3 diodes were as high as 20 foot-lamberts at a current level of 20 ma.

Thus, isoelectronic nitrogen doping has been found to be effective in increasing the blue-green light emission of (Ga,Al)P p-n junction diodes and in suppressing the deep red component found in diodes which were not nitrogen doped. Efficiencies in the blue-green of up to 4×10^{-5} were observed.

Although it is possible that a more careful investigation of the dependence of efficiency on the doping levels would further increase the efficiency of these diodes, it seems likely that substantial improvements would be found only if a drastic reduction in the "undoped" p-type background level can be made. At present, massive Te doping (~ 6×10^{19} cm^{-3} in a melt and at least 5×10^{18} cm^{-3} in the solid) is required to overcome this high background level to form the p-n junctions and it is known that nitrogen doping of GaP diodes is most effective only when the Te level is kept low.

The likelihood of success in such an endeavor is unclear since the source of this background doping is not easily elucidated. Therefore, it cannot be strongly recommended that work should be continued to further increase the light emission of such diodes.

TABLE 4

| Type	Sample	Substrate	Carrier Concentration n-layer	Carrier Concentration p-layer
I(undoped)	GLPE-65	<111> n	4×10^{17}	2×10^{18}
	-66	<111> n	2×10^{17}	2×10^{18}
	-68	<111> n	5×10^{17}	2×10^{18}
	-70	<111> n	1×10^{18}	2×10^{18}
	-72	<111> p	5×10^{17}	2×10^{18}
	-73	<111> p	2×10^{18}	2×10^{18}
	-74	<111> p	3×10^{17}	9×10^{17}
II(Zn-Te)	GLPE-75	<111> p	8×10^{17}	3×10^{18}
	-76	<111> p	3×10^{17}	3×10^{18}
	-77	<111> p	5×10^{17}	4×10^{18}
	-78	<111> p	5×10^{17}	2×10^{18}
III(Zn-Te)N	GLPE-80	<111> p	3×10^{17}	2×10^{18}
	-81	<111> p	3×10^{17}	2×10^{18}
	-83	<111> p	3×10^{17}	4×10^{18}
	-84	<111> n	5×10^{17}	2×10^{18}
	-87	<111> p	7×10^{17}	4×10^{18}
	-92	<111> p	5×10^{17}	9×10^{17}
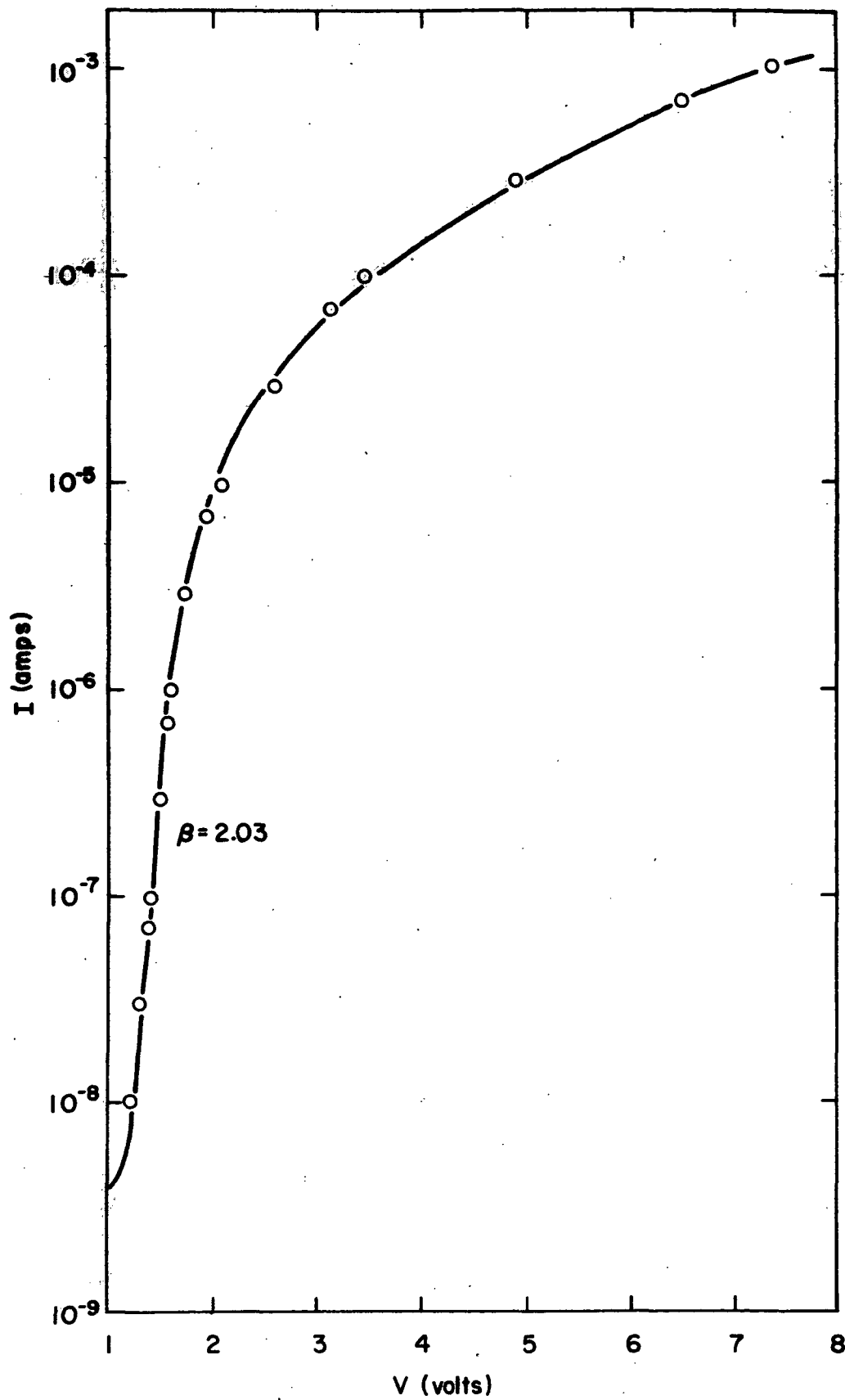
Figure 14
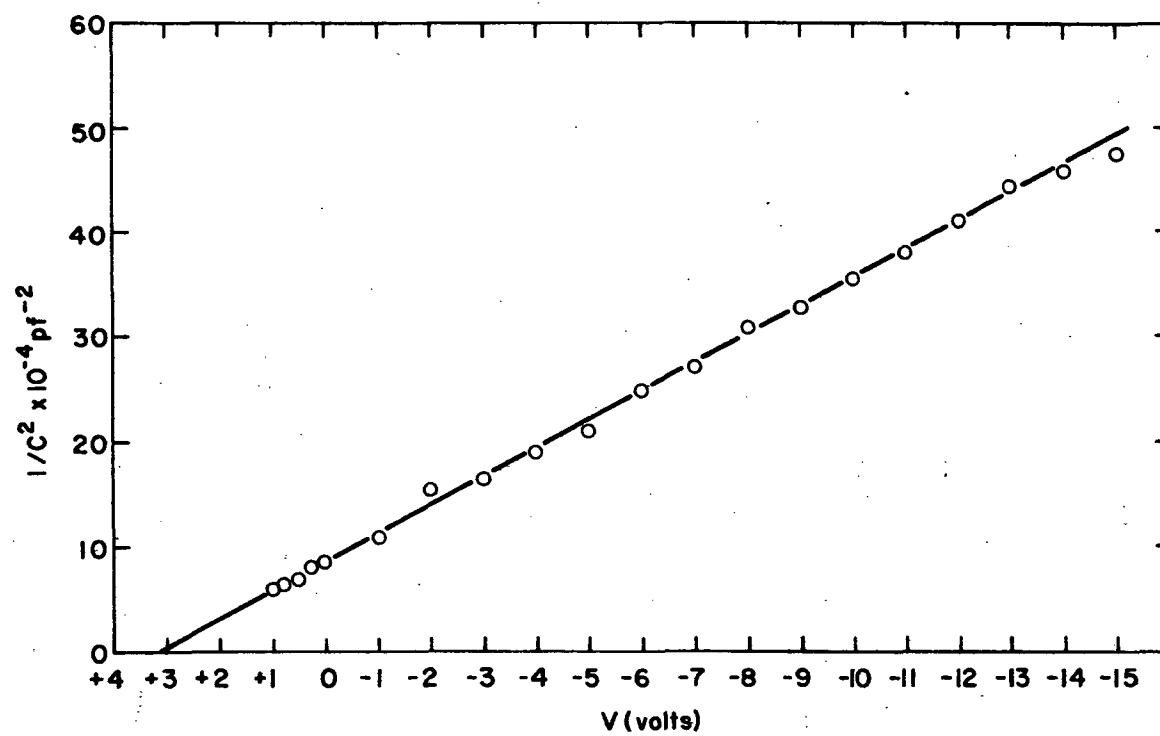
Figure 15
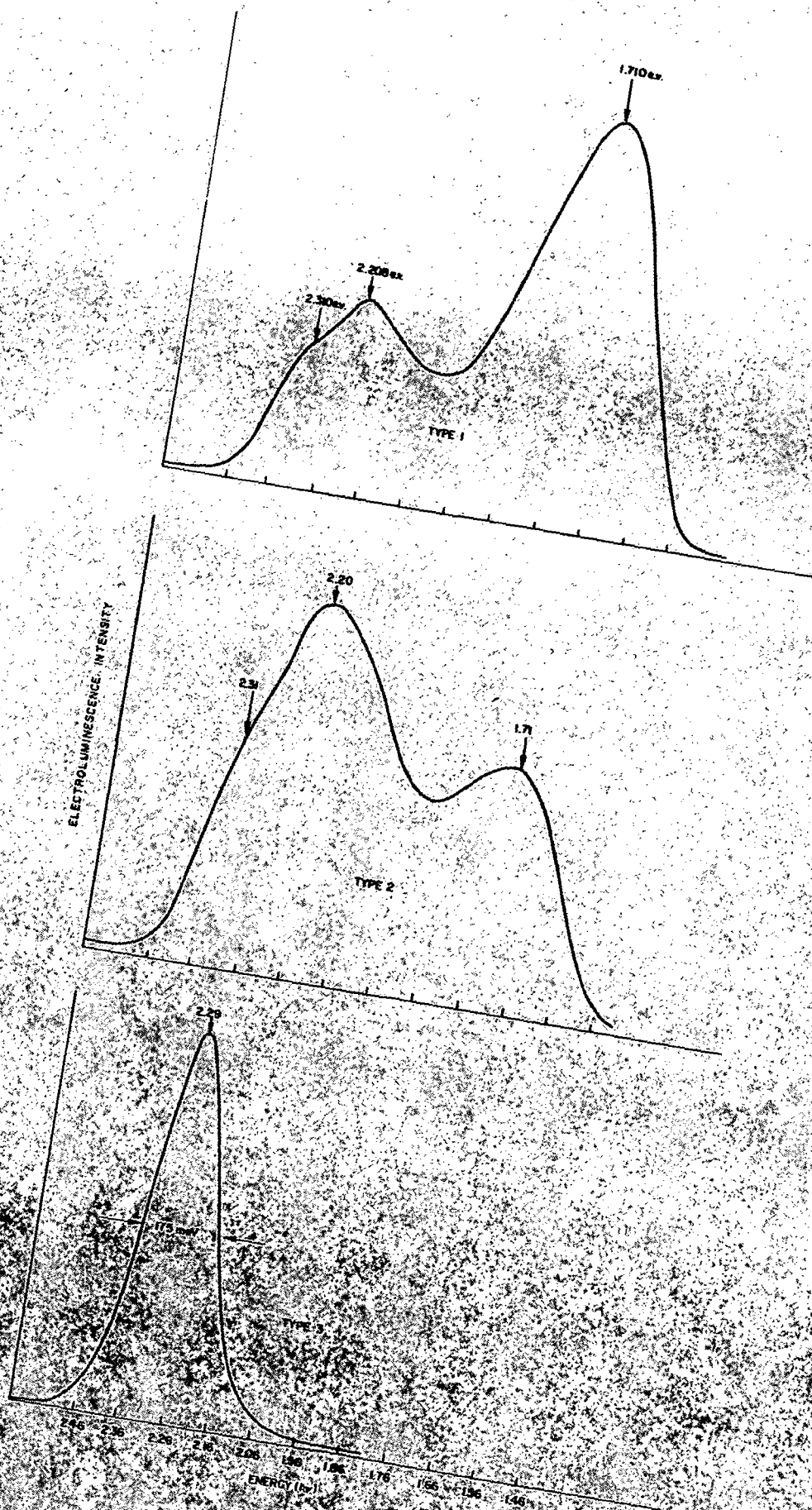
Figure 16

CONCLUSIONS AND RECOMMENDATIONS

It has been found that good control and reproducibility of the composition and composition gradients in (Ga,Al)P overgrowths can be obtained with the liquid phase epitaxy growth method. Also these overgrowth layers can be doped p-type or n-type with good control and p-n junctions can be formed by using these techniques.

These overgrowth layers have been characterized electrically and optically and these properties are reasonably well understood with the exceptions that nominally undoped layers are strongly p-type ($\sim 2 \times 10^{18}$ cm^{-3}) and that the impurity levels responsible for the observed photoluminescence and electro-luminescence have not been unambiguously established. The p-type character of the "undoped" layers is particularly important since the consequent highly compensated nature of the n-type growths is probably deleterious to obtaining high radiative efficiencies. Changes in the materials of the growth apparatus and the use of high purity starting materials did not alter this background p-doping level.

A number of p-n junction diodes have been fabricated. These were of three types: "undoped" (p)- Te(n), Zn(p)- Te(n), and Zn(p)- Te(n) plus isoelectronic nitrogen. The electrical characteristics of all three types were measured and found to be similar and under control. The results are consistent with those expected for abrupt junction diodes with recombination in the space charge region. However, the series resistance is apparently high and the forward current at a given voltage is substantially lower than might have been expected by analogy to GaP diodes.

All three diode types emitted blue-green light (h$\nu \sim 2.30$ eV) with the first two types also having a substantial deep red emission (h$\nu \sim 1.71$ eV). The nitrogen doped diodes produced blue-green light at the highest efficiency and with the red emission absent. Several of these diodes had measured efficiencies of 4×10^{-5}, with most of the diodes having efficiencies nearer 10^{-6}.

These results are encouraging in the sense that the higher frequency emission inherent in this higher band gap material has been realized and that at least reasonable efficiencies have been obtained. However, it is believed that to obtain substantially higher efficiencies it would be necessary to understand and decrease the high level of "unintentional" p-type background doping so that less tellurium would be required to form the n-layer and thus to ensure that the nitrogen doping would be more effective.

Our attempts to date to understand and reduce the p-type background level have been unsuccessful and this probably indicates that extensive additional work would be required to overcome this difficulty with the likelihood of success unclear. It is also possible, and some very rough and qualitative calculations indicate that this may be so, that nitrogen may not be as effective a re-combination center in (Ga,Al)P as it is in GaP.

Therefore, in view of these uncertainties and in view of the recent improvements made by RCA in the growth of the (GaIn)P direct band gap alloy system, it cannot be strongly recommended that work should be continued on the (Ga,Al)P alloy system.